UNDERSTANDING CONTRASTIVE LEARNING THROUGH VARIATIONAL ANALYSIS AND NEURAL NETWORK OPTIMIZATION PERSPECTIVES

Anonymous authors
Paper under double-blind review

ABSTRACT

The SimCLR method for contrastive learning of invariant visual representations has become extensively used in supervised, semi-supervised, and unsupervised settings, due to its ability to uncover patterns and structures in image data that are not directly present in the pixel representations. However, the reason for this success is not well-explained, since it is not guaranteed by invariance alone. In this paper, we conduct a mathematical analysis of the SimCLR method with the goal of better understanding the geometric properties of the learned latent distribution. Our findings reveal two things: (1) the SimCLR loss alone is not sufficient to select a *good* minimizer — there are minimizers that give trivial latent distributions, even when the original data is highly clustered — and (2) in order to understand the success of contrastive learning methods like SimCLR, it is necessary to analyze the neural network training dynamics induced by minimizing a contrastive learning loss. Our preliminary analysis for a one-hidden layer neural network shows that clustering structure can present itself for a substantial period of time during training, even if it eventually converges to a trivial minimizer. To substantiate our theoretical insights, we present numerical results that confirm our theoretical predictions.

1 INTRODUCTION

Unsupervised learning of effective representations for data is one of the most fundamental problems in machine learning, especially in the context of image data. The widely successful *discriminative approach* to learning representations of data is most similar to fully supervised learning, where features are extracted by a backbone convolutional neural network, except that the fully supervised task is replaced by an unsupervised or *self-supervised* task that can be completed without labeled training data.

Many successful discriminative representation learning methods are based around the idea of finding a feature map that is *invariant* to a set of transformations (i.e., data augmentations) that are expected to be present in the data. For image data, the transformations may include image scaling, rotation, cropping, color jitter, Gaussian blurring, and adding noise, though the question of which augmentations give the best features is not trivial (Tian et al., 2020). Invariant feature learning methods include VICReg Bardes et al. (2021), Bootstrap Your Own Latent (BYOL) (Grill et al., 2020), Siamese neural networks Chicco (2021), and contrastive learning techniques such as SimCLR Chen et al. (2020) (see also (Hadsell et al., 2006; Dosovitskiy et al., 2014; Oord et al., 2018; Bachman et al., 2019)).

In contrastive learning, the primary self-supervised task is to differentiate between positive and negative pairs of data instances. The goal is to find a feature map for which positive pairs have maximally similar features, while negative pairs have maximal different features. The positive and negative examples do not necessarily correspond to classes. In SimCLR, positive pairs are images that are the same up to a transformation, while all other pairs are negative pairs. Contrastive learning has also been successfully applied in supervised (Khosla et al., 2020) and semi-supervised contexts (Li et al., 2021; Yang et al., 2022; Singh, 2021; Zhang et al., 2022b; Lee et al., 2022; Kim et al.,

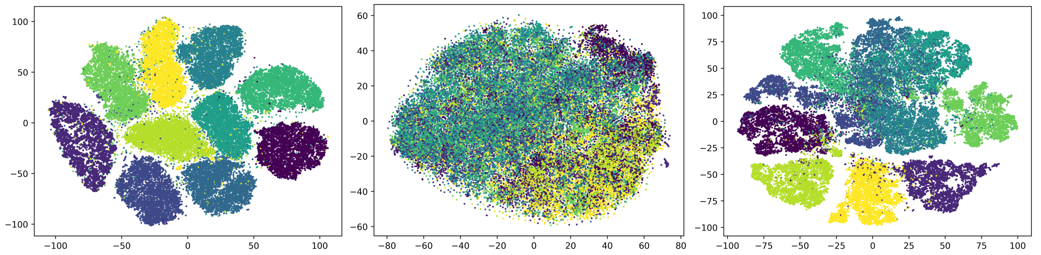

(a) MNIST: pixel space (b) Cifar10: pixel space (c) Cifar10: SimCLR

Figure 1: t-SNE visualizations of the MNIST and Cifar10 data sets. In (a) and (b) the images are represented by the raw pixels, while (c) gives a visualization of the SimCLR embedding. This illustrates how SimCLR is able to uncover clustering structure in data sets.

2021; Ji et al., 2023), and has been used for learning Lie Symmetries of partial differential equations Mialon et al. (2023) (for a survey see Le-Khac et al. (2020)).

All invariance based feature extraction techniques must address the fundamental problem of dimension collapse, whereby a method learns the trivial constant map $f(x) = c$ (or a very low rank map), which is invariant to *all* transformations, but not informative or descriptive. There are various ways to prevent dimension collapse. In contrastive learning the role of the negative pairs is to prevent collapse by creating repulsion terms in the latent space, however, full or partial collapse can still occur (Jing et al., 2021; Zhang et al., 2022a; Shen et al., 2022; Li et al., 2022). In BYOL collapse is prevented by halting backpropagation in certain parts of the loss, and incorporating temporal averaging. In VICReg, additional terms are added to the loss function to maintain variance in each latent dimension, as well as to decorrelate variables.

Provided dimensional collapse does not occur, a fundamental unresolved question surrounding many feature learning methods is: why do they work so well at producing embeddings that uncover key features and patterns in data sets? As a simple example, consider fig. 1. In fig. 1a and fig. 1b we show t-SNE (Van der Maaten & Hinton, 2008) visualizations of the MNIST (Deng, 2012) and Cifar-10 (Krizhevsky et al., 2009) data sets, respectively, using their pixel representations. We can see that visual features are not required on MNIST, which is highly preprocessed, while for Cifar-10 the pixel representations are largely uninformative, and feature representations are essential. In fig. 1c we show a t-SNE visualization of the latent embedding of the SimCLR method applied to Cifar-10, which indicates that SimCLR has uncovered a strong clustering structure in Cifar-10 that was not present in the pixel representation.

The goal of this paper is to provide a framework that can begin to address this question, and in particular, to explain fig. 1. To do this, we assume the data follows a *corruption* model, where the observed data is derived from some clean data with distribution μ that is highly structured or clustered in some way (e.g., follows the manifold assumption with a clustered density). The observed data is then obtained by applying transformations at random from a set of augmentations $\mathcal{T}$ to the clean data points (i.e., taking different views of the data), producing a corrupted distribution $\widetilde{\mu}$. The main question that motivated our work is that of understanding what properties of the original clean data distribution μ can be uncovered by unsupervised contrastive feature learning techniques? That is, once an invariant feature map $f : \mathbb{R}^D \to \mathbb{R}^d$ is learned, is the latent distribution $f_{\#}\widetilde{\mu}$ similar in any to the clean distribution μ, or can it be used to deduce any geometric or topological properties of μ?

This paper has two main contributions. For simplicity we focus on SimCLR, and indicate in the appendix how our results extend to other techniques.

1. We show minimizing the SimCLR contrastive learning loss is not sufficient to recover information about μ. In particular, there are invariant minimizers of the SimCLR loss that are completely independent of the data distributions μ and $\widetilde{\mu}$. In the extreme case, the original clean data may be highly clustered, while the latent distribution has a minimizer that is the uniform distribution.

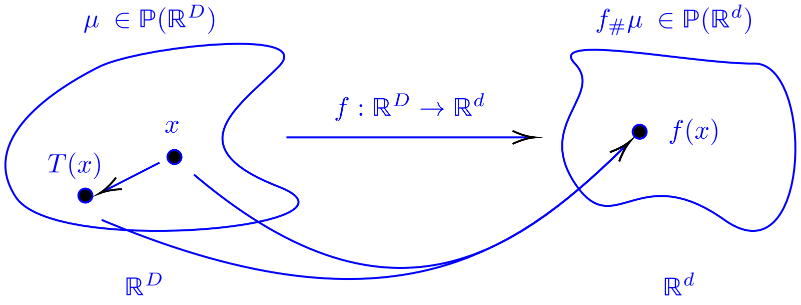
$\mu \in \mathbb{P}(\mathbb{R}^D)$
$f_\# \mu \in \mathbb{P}(\mathbb{R}^d)$
$f : \mathbb{R}^D \to \mathbb{R}^d$
x
$T(x)$
$f(x)$
$\mathbb{R}^D$
$\mathbb{R}^d$

Figure 2: ~~Illustration of T and f~~ Illustration of an invariant feature map $f : \mathbb{R}^D \to \mathbb{R}^d$ that maps the data distribution μ to the feature distribution $f_\# \mu$ in the latent space, along with a perturbation function $T : \mathbb{R}^D \to \mathbb{R}^D$. The figure shows that both the original point x and the perturbed point $T(x)$ map to $f(x)$ in the feature space.

2. To understand the success of contrastive learning, it is necessary to analyze the neural network training dynamics induced by gradient descent on the SimCLR loss. Using the neural kernel approach, we show that clusterability structures in μ strongly affect the training dynamics and can remain present in the latent distribution for a long time, even if gradient descent converges to a trivial minimizer.

Our work is complementary to work on dimension collapse in contrastive learning (Jing et al., 2021; Zhang et al., 2022a; Shen et al., 2022; Li et al., 2022), since our observations hold even when there is no collapse. We also mention there is other recent work (Meng & Wang, 2024) on understanding the training dynamics of contrastive learning through a continuum limit partial differential equation. Other related works include (HaoChen et al., 2021; Balestriero & LeCun, 2022), which provide guarantees on contrastive learning for downstream tasks, such as semi-supervised learning. The idea in these works is to define an "augmentation graph" based on the relations between positive and negative examples in contrastive learning, and study how the class-membership clusters align with the augmentation graph — when they are aligned, downstream tasks perform well. Our paper is complementary to these works, since we essentially study the question of when this alignment holds in contrastive learning.

Outline: In section 2 we overview contrastive learning, and our corruption model for the data. In section 3 we derive and study the optimality conditions for the SimCLR loss, and give conditions for stationary points. In section 4 we study the neural dynamics of training SimCLR for a one-hidden layer neural network.

2 CONTRASTIVE LEARNING

We describe here our model for corrupted data in the setting of contrastive learning, and a reformulation of the SimCLR loss that is useful or our analysis. Let $\mu \in \mathbb{P}(\mathbb{R}^D)$ be a data distribution in $\mathbb{R}^D$. Let $\mathcal{T}$ be a set of transformation functions $T : \mathbb{R}^D \to \mathbb{R}^D$ that is measurable such that, for a given $x \in \mathbb{R}^D$, $T(x) \in \mathbb{R}^D$ represents a perturbation of x, such as a data augmentation (e.g., cropping and image, etc.). Let $\widetilde{\mu} \in \mathbb{P}(\mathbb{R}^D)$ denote the distribution obtained by perturbing μ with the perturbations defined in $\mathcal{T}$. That is, we choose a probability distribution $\nu \in \mathbb{P}(\mathcal{T})$ over the perturbations, and samples from $\widetilde{\mu}$ are generated by sampling $x \sim \mu$ and $f \sim \nu$, and taking the composition $f(x)$.

We treat μ as the original clean data, which is not observable, while the perturbed distribution $\widetilde{\mu}$ is how the data is presented to the user. Our goal is to understand whether contrastive learning can recover information about the original data distribution μ, provided the distribution of augmentations ν is known.

Ostensibly, the objective of contrastive learning is to identify an embedding function $f : \mathbb{R}^D \to \mathbb{R}^d$ that is invariant to the set of transformations $\mathcal{T}$. Provided such an invariant map is identified, f

pushes forwards both μ and $\widetilde{\mu}$ to the same latent distributions, that is

$$f_{\#}\widetilde{\mu} = f_{\#}\mu.$$

As a result, the desirable map f is not only invariant to perturbations from $\mathcal{T}$ but also successfully retrieves the unperturbed data distribution μ, ensuring that the embedded distribution $f_{\#}\mu$ serves as a pure feature representation of the given data distribution. However, it is far from clear how μ and $f_{\#}\mu$ are related, and whether any interesting structures in μ (such as clusterability) are also present in $f_{\#}\mu$.

For instance, if $\widetilde{\mu}$ represents image data, contrastive learning aims to discover a feature distribution $f_{\#}\widetilde{\mu}$ that remains invariant to transformations such as random translation, rotation, cropping, Gaussian blurring, and others. Figure 2 illustrates the mapping $f : \mathbb{R}^D \to \mathbb{R}^d$ and $T \in \mathcal{T}$. As a result, this feature distribution effectively captures the essential characteristics of the data without being influenced by these perturbations. These feature distributions are often leveraged in downstream tasks such as classification, clustering, object detection, and retrieval, where they achieve state-of-the-art performance (Le-Khac et al., 2020).

To achieve this, one designs a cost function that encourages similar points to be closer together and dissimilar points to be farther apart through the embedding map, leveraging attraction and repulsion forces. One of the most popular cost functions is introduced by Chen et al. (2020), known as the Normalized Temperature-Scaled Cross-Entropy Loss (NT-Xent loss). Minimizing the NT-Xent loss leads to the optimization problem

$$\min_{f:\mathbb{R}^D\to\mathbb{R}^d} \mathop{\mathbb{E}}_{x\sim\mu, T, T'\sim\nu} \log\left(1 + \frac{\sum_{h\in\{T,T'\}} \mathbb{E}_{y\sim\mu}\left[\mathbb{1}_{x\neq y}\exp\left(\frac{\mathrm{sim}_f(T(x),h(y))}{\tau}\right)\right]}{\exp\left(\frac{\mathrm{sim}_f(T(x),T'(x))}{\tau}\right)}\right), \tag{1}$$

where $\nu \in \mathbb{P}(\mathcal{T})$ is a probability distribution on $\mathcal{T}$, which is assumed to be a measurable space, τ is a given parameter, and $\mathrm{sim}_f : \mathbb{R}^D \times \mathbb{R}^D \to \mathbb{R}$ is a function measuring the similarity between two embedded points with f in $\mathbb{R}^d$ defined as:

$$\mathrm{sim}_f(x, y) = \frac{f(x)\cdot f(y)}{\|f(x)\|\|f(y)\|}. \tag{2}$$

The denominator inside the log function acts as an attraction force between two perturbed points from the same sample x, while minimizing the numerator acts as a repulsion force between two perturbed points from two different samples x and y. As a result, the minimizer f of the cost is expected to exhibit invariance under the group of perturbation functions from ν, so that

$$f(T(x)) = f(x), \qquad \forall\, x \in \mathbb{R}^D,\ \forall\, T \in \mathcal{T}. \tag{3}$$

The repulsion force prevents dimensional collapse, where the map sends every sample to a constant: $f(x) = c$ for all $x \in \mathbb{R}^D$.

Our first observation is that the NT-Xent loss becomes independent of the data distribution once f is invariant, and so the latent distribution for an invariant minimizer may be completely unrelated to the input data.

Proposition 2.1. *Suppose $\mu \in \mathbb{P}(\mathbb{R}^d)$ is absolutely continuous and the embedding map $f : \mathbb{R}^D \to \mathbb{R}^d$ is invariant under the distribution ν, satisfying eq.* (3)*. Applying a change of variables, we obtain the following reformulation from eq.* (1)*:*

$$\begin{aligned}
&\min_{f:\mathbb{R}^D\to\mathbb{R}^d} \mathop{\mathbb{E}}_{x\sim f_{\#}\mu} \log\left(1 + 2 \mathop{\mathbb{E}}_{y\sim f_{\#}\mu}\left[\mathbb{1}_{x\neq y}\exp(\mathrm{sim}_f(x,y)/\tau)\right]\right)\\
&= \min_{\rho\in\mathbb{P}(\mathbb{R}^d)} \mathop{\mathbb{E}}_{x\sim\rho} \log\left(1 + 2 \mathop{\mathbb{E}}_{y\sim\rho}\left[\mathbb{1}_{x\neq y}\exp(\mathrm{sim}(x,y)/\tau)\right]\right),
\end{aligned}$$

where $\mathrm{sim}(x, y) = \mathrm{sim}_{\mathrm{Id}}(x, y) = \frac{x\cdot y}{\|x\|\|y\|}$.

This result in Proposition 2.1 shows that the minimization problem with respect to an embedding map under the NT-Xent cost, once the map is invariant, becomes equivalent to minimizing over the probability distribution in the latent space. Furthermore, this latter minimization problem is *completely independent* of the input data distribution μ. This phenomenon is also observable in other unsupervised learning models such as VICReg (Bardes et al., 2021) and Bootstrap Your Own Latent (BYOL) (Grill et al., 2020), for which we provide a similar derivation in the appendix.

In the subsequent sections, we will further explore the NT-Xent loss by analyzing its minimizer, as well as the dynamics of gradient descent. For this, it is useful to reformulate the loss slightly, in order to avoid the nondifferentiability of the angular similarity sim_f, and the nonuniqueness of solutions (e.g., if f is a minimizer in eq. (1), then kf for any $k > 0$ is also a minimizer). To address these issues and simplify the analysis, we consider the following generalized formulation of the NT-Xent loss in equation 1:

Definition 2.1. The cost function we consider for contrastive learning is

$$\inf_{f\in\mathcal{C}} \left\{ L(f) := \mathop{\mathbb{E}}_{x\sim\mu, T, T'\sim\nu} \Psi\left(\frac{\mathbb{E}_{y\sim\mu}\, \eta_f(T(x), T'(y))}{\eta_f(T(x), T'(x))} \right) \right\}, \tag{4}$$

where $\Psi : \mathbb{R} \to \mathbb{R}$ is a nondecreasing function, $\mathcal{C}$ is a constraint set, and η_f is defined as

$$\eta_f(x, y) = \eta(\|f(x) - f(y)\|^2/2), \tag{5}$$

where $\eta : \mathbb{R}_{\geq 0} \to \mathbb{R}$ is a differentaible similarity function that is maximized at 0.

The formulation in eq. (4) generalizes the original formulation in eq. (1) by removing the indicator function $\mathbb{1}_{x\neq y}$, as the effect of this function becomes negligible when a large n is considered. Furthermore, the generalized formulation introduces a differentaible similarity function. This simplifies the analysis of the minimizer in the variational formulation. The generalized formulation can easily be related to the original cost function in eq. (1) by setting $\Psi(t) = \log(1 + t)$, $\eta(t) = e^{-t/\tau}$ and defining $\mathcal{C} = \{f : \mathbb{R}^D \to \mathbb{S}^{d-1}\}$. Then, the similarity function η_f retains the same interpretation as angular similarity sim_f. This is because, if f lies on the unit sphere in $\mathbb{R}^d$, and so

$$\exp\left(-\frac{1}{2\tau}\|f(x) - f(y)\|^2\right) = \exp\left(\frac{1}{\tau}(f(x)\cdot f(y) - 1)\right) = C\exp\left(\frac{1}{\tau}\frac{f(x)\cdot f(y)}{\|f(x)\|\|f(y)\|}\right),$$

where $C = \exp(-1/\tau)$. The consideration of the constraint also resolves the issue in eq. (1), where kf, for any $k \in \mathbb{R}$, could be a minimizer, given a minimizer f of eq. (1). Thus, in the end, the introduced formulation in eq. (4) remains fundamentally consistent with the original NT-Xent cost structure.

3 OPTIMALITY CONDITION

In this section, we aim to find the optimality condition for the contrastive learning problem equation 4 and analyze properties of the minimizers. Our first result provides the first order optimality conditions.

Proposition 3.1. *The first optimality condition of the problem eq.* (4) *takes the form*

$$\begin{aligned}\int_{\mathcal{T}}\int_{\mathbb{R}^D} \Big\langle \int_{\mathcal{T}}\int_{\mathbb{R}^D} &\left(\frac{\Psi'(G_{T,T'}(f,x))}{\eta_f(T(x),T'(x))} + \frac{\Psi'(G_{T,T'}(f,y))}{\eta_f(T(y),T'(y))}\right)\eta_f'(T(x),T'(y))\big(f(T(x)) - f(T'(y))\big)\\ &- \big(\Psi'(G_{T,T'}(f,x))\eta_f(T(x),T'(y)) + \Psi'(G_{T',T}(f,x))\eta_f(T'(x),T(y))\big)\\ &\frac{\eta_f'(T(x),T'(x))}{\eta_f^2(T(x),T'(x))}\big(f(T(x)) - f(T'(x))\big)d\mu(y)d\nu(T'), h(T(x))\Big\rangle d\mu(x)d\nu(T) = 0\end{aligned} \tag{6}$$

for all h such that $f + h \in \mathcal{C}$ where $\eta_f'(x,y) = \eta'(\|f(x) - f(y)\|^2/2)$, $\Psi(t) = \log(1+t)$ and $G_{T,T'}(f,x) = \frac{\mathbb{E}_{z\sim\mu}\eta_f(T(x),T'(z))}{\eta_f(T(x),T'(x))}$.

If f is invariant to the perturbation in ν, then the gradient of L takes the form

$$\nabla L(f)(x) = \int_{\mathbb{R}^D} \left(\Psi'(G(f,x)) + \Psi'(G(f,y))\right)\eta_f'(x,y)(f(x) - f(y))d\mu(y) \tag{7}$$

where $G(f,x) = G_{\mathrm{Id},\mathrm{Id}}(f,x)$.

Using the first optimality condition described in Proposition 3.1, we can characterize the minimizer of the NT-Xent loss in eq. (4). The following theorem describes the possible local minimizers of eq. (4), considering the constraint set defined as $\mathcal{C} = \{f : \mathbb{R}^D \to \mathbb{S}^{d-1}\}$.

Theorem 3.2. *Given a data distribution* $\mu \in \mathbb{P}(\mathbb{R}^D)$*, let* $f \in \mathcal{C} = \{f : \mathbb{R}^D \to \mathbb{S}^{d-1}\}$ *be an invariant map such that the embedded distribution* $f_\# \mu$ *is a symmetric discrete measure satisfying*

$$\int_{\mathbb{S}^{d-1}} h(x_1, y) df_\# \mu(y) = \int_{\mathbb{S}^{d-1}} h(x_2, y) df_\# \mu(y), \tag{8}$$

for all $x_1, x_2 \sim f_\# \mu$ *and for all anti-symmetric functions* $h : \mathbb{S}^{d-1} \times \mathbb{S}^{d-1} \to \mathbb{S}^{d-1}$ *such that* $h(x, y) = -h(y, x)$*. Then,* f *is a stationary point of eq.* (4) *in* $\mathcal{C}$*.*

Remark 3.1. Examples of the embedded distribution $f_\# \mu$ described in Theorem 3.2 include a discrete measure, where $f_\# \mu = \frac{1}{n} \sum_{i=1}^{n} \delta_{x_i}$, and the points x_i are evenly distributed on $\mathbb{S}^{d-1}$. This also includes the case where all points are mapped to a single point, $f_\# \mu = \{x\}$. Figure 3 shows plots of the loss for different embedded distributions $f_\# \mu = \frac{1}{K} \sum_{i=1}^{K} \delta_{x_i}$, with the points x_i evenly distributed on $\mathbb{S}^1$, illustrating how each stationary point relates to the loss function.

In the first plot, the loss is shown as a function of the number of clusters. As the number of clusters increases, the loss decreases, but eventually reaches a point where further increases no longer reduce it. Similarly, the second plot shows the loss as a function of the minimum squared distance between two cluster points, x_i and x_j. As the distance between cluster points decreases, the loss also decreases, but it stops decreasing once the minimum squared distance reaches a threshold. Both results suggest that for a given value of τ, selecting an embedded distribution with a high number of clusters or a uniform distribution on $\mathbb{S}^1$ can minimize the NT-Xent loss function. Additionally, increasing the number of cluster points and simultaneously decreasing the value of τ can further reduce the NT-Xent loss, as clearly illustrated in the figures.

The third plot shows the relationship between τ and the threshold for the minimum squared distance between two cluster points, where the loss ceases to decrease. The main purpose of this plot is to provide insight into the optimal cluster structure of the embedded distribution that minimizes the loss for a given value of τ. The results suggest that the minimum squared distance between two cluster points and τ are linearly related.

Remark 3.2. Theorem 3.2 is related to the result from Wang & Isola (2020), where the authors studied a possible local minimizer based on minimizing the repulsive force under the assumption of an invariant feature map. In their work, they showed that, asymptotically, as the number of negative points approaches ∞, the uniform distribution on $\mathbb{S}^{d-1}$ satisfies the local minimizer. Our result extends this by providing a more general characterization of local minimizers, and unlike their result, it is not asymptotic. In this sense, our work generalizes their findings and offers a broader perspective on the possible local minimizers.

It follows from Theorem 3.2 that gradient descent on the NT-Xent loss can lead to solutions that are *completely independent* of the original data distribution μ. For instance, if μ has some underlying cluster structure, with multiple clusters, there are minimizers of the NT-Xent loss, i.e., an invariant map f, that map onto an *arbitrary* distribution in the latent space, completely independent of the clustering structure of μ. However, in practice, when the map is parameterized using neural networks, and trained with gradient descent on $L(f)$, it is very often observed that the clustering structure of the original data distribution μ emerges in the latent space (see fig. 1). In fact, our results in section 4 show that this is true even if we initialize gradient descent very poorly, starting with an invariant f mapping to the uniform distribution $\mathcal{U}(\mathbb{S}^{d-1})$!

Thus, even though the contrastive loss $L(f)$ has minimizers that ignore the data distribution μ, and thus would give poor results, when contrastive learning is trained in practice the results are often extremely good. This indicates that the parameterization of f with a neural network and the subsequent optimization via gradient descent are *selecting* a good minimizer to $L(f)$, which produces, for example, highly clustered distributions in the latent space. In order to understand this, we need to analyze the dynamics of neural network optimization during training. In the following sections, we will explore the minimization problem through this lens.

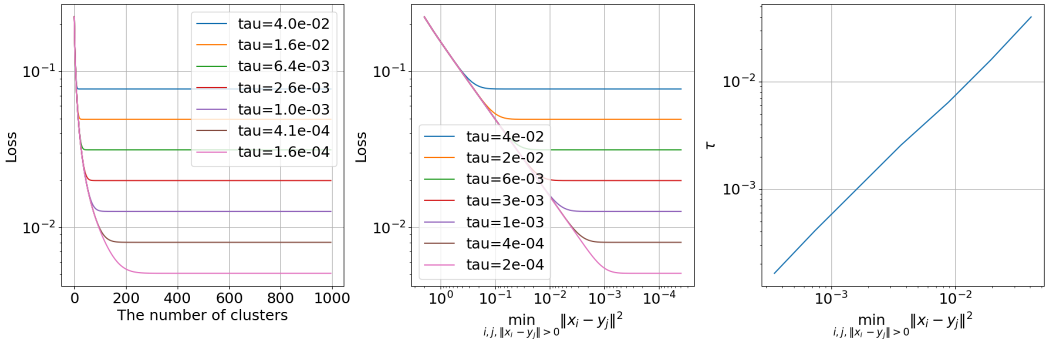

Figure 3: The figure shows the NT-Xent loss for different stationary points, represented by various embedded distributions $f_{\#}\mu = \frac{1}{K}\sum_{i=1}^{K} \delta_{x_i}$, where the x_i are evenly distributed on $\mathbb{S}^1$. The first plot demonstrates the loss decreasing as the number of clusters increases, until it reaches a point where further increases no longer reduce the loss. The second plot shows the loss decreasing with the minimum squared distance between cluster points decreasing, and stopping once a threshold is reached. Both plots suggest that increasing the number of clusters and decreasing τ can reduce the NT-Xent loss. The third plot illustrates a linear relationship between τ and the threshold for the minimum squared distance, indicating the optimal cluster structure for minimizing loss.

4 OPTIMIZATION OF NEURAL NETWORKS

Here, we study contrastive learning through the lens of the associated neural network training dynamics, which illustrates how the data distribution enters the latent space through the neural kernel. In this section, we use the notation $\llbracket n \rrbracket = \{1, \dots, n\}$.

4.1 GRADIENT FLOW FROM NEURAL NETWORK PARAMETERS

Let $w \in \mathbb{R}^m$ be a vector of neural network parameters, $\{x_1, \dots, x_n\} \subset \mathbb{R}^D$ be data samples, and $f(w, x_i) = (f^1(w, x_i), \dots, f^d(w, x_i))^\top \in \mathbb{R}^d$ be an embedding function where each function $f^k : \mathbb{R}^{n+D} \to \mathbb{R}$ is a scalar function for $k = 1, \dots, d$. Consider a loss function $L = L(y^1, \cdots, y^d) : \mathbb{R}^d \to \mathbb{R}$ with respect to w:

$$\mathcal{L}(w) = \frac{1}{n} \sum_{i=1}^{n} L(f(w, x_i)). \tag{9}$$

Let $w(t)$ be a vector of neural network parameters as a function of time t. The gradient descent flow can be expressed as

$$\dot{w}(t) = -\nabla \mathcal{L}(w).$$

Due to the highly non-convex nature of $\mathcal{L}$, this gradient flow is difficult to analyze. By shifting the focus to the evolution of the neural network's output on the training data over time, rather than the weights, we can derive an alternative gradient flow with better properties for easier analysis. The following proposition outlines this gradient flow derived from the loss function $\mathcal{L}$. The proof of the proposition is provided in the appendix.

Proposition 4.1. *Let $w(t)$ be a vector of neural network parameters as a function of time t. Consider a set of data samples $\{x_1, \dots, x_n\}$. Define a matrix function $z : \mathbb{R} \to \mathbb{R}^{d \times n}$ such that*

$$z(t) = \begin{pmatrix} f^1(w(t), x_1) & f^1(w(t), x_2) & \cdots & f^1(w(t), x_n) \\ f^2(w(t), x_1) & f^2(w(t), x_2) & \cdots & f^2(w(t), x_n) \\ \vdots & \vdots & \ddots & \vdots \\ f^d(w(t), x_1) & f^d(w(t), x_2) & \cdots & f^d(w(t), x_n) \end{pmatrix}. \tag{10}$$

Let z_i denote the i-th column of z. Then, $z_i(t)$ satisfies the following ordinary differential equation (ODE) for each $i \in \llbracket n \rrbracket$:

$$\dot{z}_i(t) = -\frac{1}{n} \sum_{j=1}^{n} K_{ij}(t) \nabla L(z_j(t)) \in \mathbb{R}^d, \tag{11}$$

where the kernel matrix $K_{ij} \in \mathbb{R}^{d\times d}$ *is given by*

$$(K_{ij}(t))^{kl} = K_{ij}^{kl}(t) = (\nabla_w f^k(w(t), x_i))^\top (\nabla_w f^l(w(t), x_j)). \tag{12}$$

Remark 4.1. We remark that the viewpoint in proposition 4.1, of lifting the training dynamics from the neural network weights to the function space setting, is the same that is taken by the Neural Tangent Kernel (NTK) Jacot et al. (2018). The difference here is that we do not consider an *infinite width* neural network, and we evaluate the kernel function on the training data, so the results are stated with kernel matrices that are data dependent (which is important in what follows). In fact, it is important to note that proposition 4.1 is very general and holds for any parameterization of f, e.g., we have so far not used that f is a neural network.

Remark 4.2. The training dynamics in the absence of a neural network can be expressed as

$$\dot{z}_i(t) = -\nabla L_i(z_i(t)) \in \mathbb{R}^d \tag{13}$$

where K_{ij} is set to be identity matrices. In contrast to eq. (11), the above expression shows that the training dynamics on the i-th point z_i are influenced solely by the gradient of the loss function at x_i, and there is no mixing of the data via the neural kernel K (since here it is the identity matrix).

Using proposition 4.1 we can study the invariance-preserving properties (or lack thereof) of gradient descent with and without the neural network kernel.

Theorem 4.2. *Consider the gradient descent iteration from a gradient flow without a neural network in eq.* (13)*, where* $z_i^{(b)} = f(w^{(b)}, x_i)$ *for all* $i \in [\![n]\!]$*, and*

$$z_i^{(b+1)} = z_i^{(b)} - \sigma \nabla L(z_i^{(b)}), \tag{14}$$

with σ *as the step size. If* $f(w^{(0)}, \cdot)$ *is invariant to perturbations from* ν*, as defined in eq.* (17)*, then* $f(w^{(b)}, \cdot)$ *remains invariant for all gradient descent iterations.*

On the other hand, in the case of a gradient descent iteration from eq. (10)*,*

$$z_i^{(b+1)} = z_i^{(b)} - \frac{\sigma}{n} \sum_{j=1}^{n} K_{ij}^{(b)} \nabla L(z_j^{(b)}), \tag{15}$$

the invariance of f *at the* $(b+1)$*-th iteration holds only if* f *is already invariant at the b-th iteration and additionally satisfies the condition* $\nabla_w f(w^{(b)}, f(x)) = \nabla_w f(w^{(b)}, x)$ *for all* $x \in \mathbb{R}^D$ *and* $T \in \mathcal{T}$*.*

Theorem 4.2 highlights the key difference between optimization with and without neural networks. In standard gradient descent, as in eq. (14), without the neural network kernel matrix K_{ij}, the map f remains invariant throughout the entire training process, provided it is invariant at the initial time. However, in the more realistic setting of gradient descent with the neural kernel in eq. (15), even if f is initially invariant to perturbations from ν, it requires an additional condition on $\nabla_w f$ to preserve this invariance. The gradient descent in eq. (15) does not guarantee that this condition is satisfied throughout the iterations. As a result, the optimization may introduce changes that cause f to lose its invariance, leading to dynamics significantly different from those in eq. (14).

Many other works have shown that the neural kernel imparts significant changes on the dynamics of gradient descent. For example, Xu et al. (2019a;b) established the frequency principle, showing that the training dynamics of neural networks are significantly biased towards low frequency information, compared to vanilla gradient descent.

4.2 STUDYING A CLUSTERED DATASET

In this section, we explore how the neural network kernel matrix K_{ij} in eq. (12) influences the gradient flow on the contrastive learning loss. For clarity, we use a simplified setting that is straightforward enough to provide insights into the neural network's impact on the optimization process. Although simplified, the setting can be easily generalized to extend these insights to broader contexts.

Dataset Description Consider a data distribution $\mu \in \mathbb{P}(\mathcal{M})$, where $\mathcal{M}$ is a d-dimensional compact submanifold in $\mathbb{R}^D$, and a noisy data distribution $\widetilde{\mu} \in \mathbb{P}(\mathbb{R}^D)$ defined by

$$\widetilde{\mu} = \mu + \alpha,$$

where $\alpha \in \mathbb{P}(\mathcal{M}^\perp)$ represents noise (or perturbation) applied to μ in the orthogonal direction to $\mathcal{M}$.

For simplicity, assume that

$$\mathcal{M} \subset \left\{ x = (x^1, x^2, \cdots, x^d, 0, \cdots, 0) \in \mathbb{R}^D \right\},$$
$$\mathcal{M}^\perp \subset \left\{ x = (0, \cdots, 0, x^{d+1}, x^{d+2}, \cdots, x^D) \in \mathbb{R}^D \right\}.$$

Now, let's impose a clustered structure on the dataset. Given a dataset $\{x_i\}_{i=1}^n$ with n samples i.i.d. from the noisy distribution $\widetilde{\mu}$, we assume that the data is organized into N ($N \leq d$) clusters. Let $\{\xi_q\}_{q=1}^N$ be N points in $\mathcal{M}$ such that $\xi_q \cdot \xi_{q'} \neq 0$ if $q = q'$, and 0 otherwise. Suppose the data samples are arranged such that for each $i \in \{1, \dots, n\}$,

$$x_i = \xi_q + \epsilon_i \quad \text{for } n_{q-1} + 1 \leq i \leq n_q \tag{16}$$

where $0 = n_0 < n_1 < \cdots < n_N = n$ and ϵ_i is a random variable (i.e., noise) and $\|\epsilon_i\| < \delta$ for some positive constant $\delta > 0$. This setup ensures that each data point x_i lies within a ball of radius δ centered at one of the points ξ_q, effectively representing the dataset as N clusters.

Embedding Map Description Let $f : \mathbb{R}^{m+D} \to \mathbb{R}^d$ be an embedding map parameterized by a neural network, such that $f = f(w(t), x)$, where $w : \mathbb{R} \to \mathbb{R}^m$ is a vector of neural network parameters. We assume that at $t = 0$, f satisfies

$$f(w(0), x) = R(x^1, \dots, x^d, 0, \dots, 0) \in \mathbb{R}^d, \tag{17}$$

for all $x = (x^1, \dots, x^D) \in \mathbb{R}^D$, where $R : \mathbb{R}^D \to \mathbb{R}^d$ is an arbitrary map. Consequently, this embedding map f is invariant under the following perturbations: for $x \sim \mu$ and $\epsilon \sim \alpha$,

$$f(w(0), x + \epsilon) = R(x) = f(w(0), x).$$

Thus, f is an invariant to the perturbation from α. This serves to initialize the embedding map f to be an invariant map that is unrelated to the data distribution μ. This is in some sense the "worst case" initialization, where no information from the data distribution μ has been imbued upon the latent distribution. The goal is to examine what happens when using this as the initialization for training. As we will see below, the neural kernel always injects information from μ into the optimization procedure, and can even help recover from poor initializations.

4.2.1 PROPERTIES OF THE EMBEDDING MAP

In this section, we derive the explicit formulations for the gradients and the kernel matrix defined in eq. (12), within the setting described in Section 4.2. We examine the training dynamics of eq. (10) to understand how they are influenced by the neural network kernel matrix K_{ij} and the dataset's clustering structure. Specifically, we consider the embedding map $f : \mathbb{R}^{MDd+D} \to \mathbb{R}^d$ parameterized by a one-hidden-layer fully connected neural network:

$$f(w(t), x) = f(B(t), x) = A^\top \sigma(B(t)x), \tag{18}$$

where $A \in \mathbb{R}^{Md \times d}$ is a constant matrix defined as

$$A = \frac{1}{\sqrt{M}} \begin{pmatrix} \mathbb{1}_{M\times 1} & \mathbb{0}_{M\times 1} & \cdots & \mathbb{0}_{M\times 1} \\ \mathbb{0}_{M\times 1} & \mathbb{1}_{M\times 1} & \cdots & \mathbb{0}_{M\times 1} \\ \vdots & \vdots & \ddots & \vdots \\ \mathbb{0}_{M\times 1} & \mathbb{0}_{M\times 1} & \cdots & \mathbb{1}_{M\times 1} \end{pmatrix} \in \mathbb{R}^{Md\times d}, \tag{19}$$

where $\mathbb{1}_{M\times 1}$ and $\mathbb{0}_{M\times 1}$ represent the M-dimensional vectors of ones and zeros, respectively. Additionally, $B(t) = (b_p^k(t))_{k\in[\![D]\!], p\in[\![Md]\!]} \in \mathbb{R}^{Md\times D}$ is the weight matrix, and σ is a differentiable activation function applied element-wise.

Note that A acts as an averaging matrix that, when multiplied by the (Md)-dimensional vector $\sigma(B(t)x)$, produces a d-dimensional vector. Furthermore, we assume that the parameters of W are uniformly bounded, such that there exists a constant C with $|b_p^k(t)| < C$ for all $t \geq 0$, k, and p.

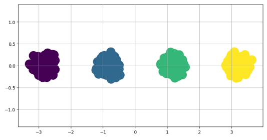

(a) Input data

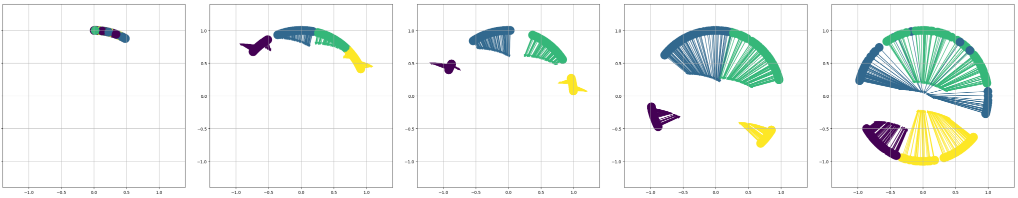

(b) It: 0 (c) It: 15 (d) It: 30 (e) It: 70 (f) It:200

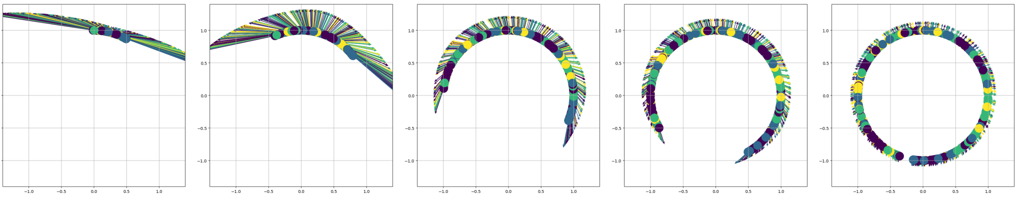

(g) It: 0 (h) It:30 (i) It: 200 (j) It: 400 (k) It: 1,000

Figure 4: Comparison of the optimization process with and without neural network training, where the data distribution is indicated in (a). The color of each point represents its corresponding cluster, and the arrow represents the negative of unit gradient at that point. Row 2 illustrates the optimization with neural network training, starting from a random initial embedding and revealing the clustering structure over iterations. Row 3 shows the optimization process using vanilla gradient descent without neural network training from the same initial embedding. As the iterations progress, the distribution converges to a uniformly dispersed arrangement, disregarding the clustering structure of the input data.

Remark 4.3. In many contrastive learning works, the neural network is trained, and the last layer is discarded when retrieving the feature representation. many works Bordes et al. (2023); Gui et al. (2023); Wen & Li (2022) studied this phenomenon in depth and found that discarding the last layer actually improves the quality of the feature representation. In this paper, we do not consider discarding the last layer for simplicity in our analysis, but it is an interesting direction for future work to explore how the last layer of the neural network affects the training dynamics.

Based on the definitions of kernel matrices in eq. (12) and the neural network function f in eq. (18), the following proposition provides the explicit kernel formula.

Proposition 4.3. *Given the description of the embedding map in eq.* (18)*, the kernel matrix* K_{ij}^{kl} *defined in eq.* (12) *can be explicitly written as*

$$K_{ij}^{kl} = \frac{\mathbb{1}_{k=l}}{M} x_i^\top x_j \sum_{p=(k-1)M+1}^{kM} \sigma'(b_p x_i)\sigma'(b_p x_j). \tag{20}$$

where $\mathbb{1}_{k=l}$ *is an indicator function that equals* 1 *if* $k = l$ *and* 0 *otherwise.*

From Proposition 4.3, as done in NTK paper (Jacot et al., 2018), one can consider how the kernel converges as the width of the neural network approaches infinity, i.e., as $M \to \infty$ in eq. (18). The following proposition shows the formulation of the limiting kernel in the infinite-width neural network.

Proposition 4.4. *Suppose the weight matrix* B *satisfies that each row vector* b_i*, for* $i \in \{1, \ldots, Md\}$*, consists of independent and identically distributed random variables in* $\mathbb{R}^D$ *with a Gaussian distribution. Also, suppose the activation function is* $\sigma(x) = x_+ = \max\{x, 0\}$*. Then, as*

$M \to \infty$, the kernel matrix converges to $K^{\infty} \in \mathbb{R}^{d\times d}$, where

$$K^{\infty}_{ij} = (x_i^\top x_j)\left[\frac{1}{2} - \frac{1}{2\pi}\arccos\left(\frac{x_i^\top x_j}{\|x_i\|\|x_j\|}\right)\right]\boldsymbol{I}_{d\times d}.$$

where $\boldsymbol{I}_{d\times d}$ is an identity matrix.

Using the kernel matrix defined in Proposition 4.3, the following theorem presents the explicit form of the gradient flows in terms of the clustering structure and the neural network parameters.

Theorem 4.5. *Let the dataset to be clustered be as described in eq.* (16). *Define a function $\gamma : [\![n]\!] \to [\![N]\!]$ such that $\gamma(i) = q$ if x_i is from the cluster point ξ_q. Then, the gradient flow formulation takes the form*

$$\dot{z}_i(t) = -\left(\frac{n_{\gamma(i)} - n_{\gamma(i)-1}}{n}\right)\|\xi_{\gamma(i)}\|^2\boldsymbol{\beta}_{\gamma(i)}\nabla L(w(t), \xi_{\gamma(i)}) + O(\delta) \qquad (21)$$

where $\boldsymbol{\beta}_q \in \mathbb{R}^{d\times d}$ ($q \in [\![n]\!]$) is a diagonal matrix where each diagonal entry $\beta_i^k \in \mathbb{R}$ ($k \in [\![d]\!]$) is defined as $\beta_q^k = \frac{1}{M}\sum_{p=(k-1)M+1}^{kM}\sigma'(b_p\xi_q)^2$.

Similar to Proposition 4.4, one can consider the gradient flow formulation in the limit of infinite width, i.e., as $M \to \infty$. The following corollary provides the explicit form of the neural network gradient flow in the infinite width case.

Corollary 4.6. *Under the same conditions as in Proposition 4.4 and Theorem 4.5, if the width approaches infinity, i.e., $M \to \infty$, then the gradient formulation in eq.* (21) *becomes*

$$\dot{z}_i(t) = -\left(\frac{n_{\gamma(i)} - n_{\gamma(i)-1}}{2n}\right)\|\xi_{\gamma(i)}\|^2\nabla L(f(w(t), \xi_{\gamma(i)})) + O(\delta).$$

Remark 4.4. The results from Theorem 4.5 and Proposition 4.4 show the explicit gradient flow under the clustering setting, where the gradient is scaled by the ratio of each cluster's size represented as $(n_{\gamma(i)} - n_{\gamma(i)-1})/n$. This means that if a certain cluster contains only a small number of points, the gradient at those points could be negligible compared to the gradient from a cluster with a larger number of points, which may result in the failure to capture the smaller cluster effectively. This result aligns well with the findings in Assran et al. (2022), where the authors show that semi-supervised methods, including contrastive learning, tend to perform worse with imbalanced class data and work better with uniform class distributions.

The formulations of the gradient flow in Theorem 4.5 and Corollary 4.6 can be viewed as a modification of the training dynamics of the vanilla gradient flow in eq. (13), altered in such a way as to steer the iterations towards a stationary solution that is both invariant to perturbations *and* influenced by the dataset's geometry. Specifically, the first term in eq. (21) shows that for every data point x_i that originates from the same cluster, the gradient will be the same, with an error of order $O(\delta)$. This means that if the neural network is initialized randomly, such that the embeddings from the feature map are completely random in the latent space, the gradient at points from the same cluster in the embedded space will follow the same direction. This results in training dynamics that lead to embeddings that exhibit the data's clustering structure.

This behavior is reflected in the numerical results in Figure 4, where a 2D dataset with four clusters located along the x-axis at -3 (purple), -1 (blue), 1 (green), and 3 (yellow) is analyzed. The arrow at each point indicates the negative gradient computed at that point. In the figure, the number of iterations is chosen differently for each training dynamic (with and without neural network optimization) because the neural network kernel matrix affects the training dynamics, causing the models to converge at different speeds. The iterations in the visualization are selected to best capture and effectively depict the evolution of the feature distribution during training. Furthermore, both figures stabilize after a certain number of iterations: the first (b-f), with neural network optimization, after 200 iterations, and the second (g-k), without it, after 1,000 iterations.

The training dynamics show that, despite starting from a random initialization without any initial clustering structure, data points from the same cluster follow a similar gradient. This shared gradient, relative to their respective clusters, drives the separation of data points from different clusters in the early iterations. By iteration 15, the clustering structure of the input data is already preserved in the embedded distribution, after just a few iterations. In contrast, without neural network optimization, the embedded data points spread out and eventually form a uniform distribution on a sphere, disregarding the input data's cluster structure. This result aligns with the theoretical findings in Theorem 3.2, which suggest that the gradient of the loss function is independent of the input data's structure.

5 CONCLUSION AND FUTURE WORK

We have studied the SimCLR contrastive learning problem from the perspective of a variational analysis and through the dynamics of training a neural network to represent the embedding function. Our findings strongly suggest that in order to fully understand the representation power of contrastive learning, it is necessary to study the training dynamics of gradient descent, as vanilla gradient descent *forgets* all information about the data distribution.

The results in this paper are preliminary, and there are many interesting directions for future work. It would be natural to examine a mean field limit (Mei et al., 2018) for the training dynamics, which may shed more light on this phenomenon (e.g., in theorem 4.5). We can also consider an infinite width neural network, as is done in the NtK setting, in theorem 4.5 to attempt to rigorously establish convergence of the training dynamics. It would also be interesting to explore applications of these techniques to other deep learning methods.

REFERENCES

Mahmoud Assran, Randall Balestriero, Quentin Duval, Florian Bordes, Ishan Misra, Piotr Bojanowski, Pascal Vincent, Michael Rabbat, and Nicolas Ballas. The hidden uniform cluster prior in self-supervised learning. *arXiv preprint arXiv:2210.07277*, 2022.

Philip Bachman, R Devon Hjelm, and William Buchwalter. Learning representations by maximizing mutual information across views. *Advances in neural information processing systems*, 32, 2019.

Randall Balestriero and Yann LeCun. Contrastive and non-contrastive self-supervised learning recover global and local spectral embedding methods. *Advances in Neural Information Processing Systems*, 35:26671–26685, 2022.

Adrien Bardes, Jean Ponce, and Yann LeCun. Vicreg: Variance-invariance-covariance regularization for self-supervised learning. *arXiv preprint arXiv:2105.04906*, 2021.

Florian Bordes, Randall Balestriero, Quentin Garrido, Adrien Bardes, and Pascal Vincent. Guillotine regularization: Why removing layers is needed to improve generalization in self-supervised learning. *Transactions on Machine Learning Research*, 2023. ISSN 2835-8856. URL `https://openreview.net/forum?id=ZgXfXSz51n`.

Ting Chen, Simon Kornblith, Mohammad Norouzi, and Geoffrey Hinton. A simple framework for contrastive learning of visual representations. In *International conference on machine learning*, pp. 1597–1607. PMLR, 2020.

Davide Chicco. Siamese neural networks: An overview. *Artificial neural networks*, pp. 73–94, 2021.

Li Deng. The mnist database of handwritten digit images for machine learning research. *IEEE Signal Processing Magazine*, 29(6):141–142, 2012.

Alexey Dosovitskiy, Jost Tobias Springenberg, Martin Riedmiller, and Thomas Brox. Discriminative unsupervised feature learning with convolutional neural networks. *Advances in neural information processing systems*, 27, 2014.

Jean-Bastien Grill, Florian Strub, Florent Altché, Corentin Tallec, Pierre Richemond, Elena Buchatskaya, Carl Doersch, Bernardo Avila Pires, Zhaohan Guo, Mohammad Gheshlaghi Azar, et al. Bootstrap your own latent-a new approach to self-supervised learning. *Advances in neural information processing systems*, 33:21271–21284, 2020.

Yu Gui, Cong Ma, and Yiqiao Zhong. Unraveling projection heads in contrastive learning: Insights from expansion and shrinkage. *arXiv preprint arXiv:2306.03335*, 2023.

Raia Hadsell, Sumit Chopra, and Yann LeCun. Dimensionality reduction by learning an invariant mapping. In *2006 IEEE computer society conference on computer vision and pattern recognition (CVPR'06)*, volume 2, pp. 1735–1742. IEEE, 2006.

Jeff Z HaoChen, Colin Wei, Adrien Gaidon, and Tengyu Ma. Provable guarantees for self-supervised deep learning with spectral contrastive loss. *Advances in Neural Information Processing Systems*, 34:5000–5011, 2021.

Arthur Jacot, Franck Gabriel, and Clément Hongler. Neural tangent kernel: Convergence and generalization in neural networks. *Advances in neural information processing systems*, 31, 2018.

Wenlong Ji, Zhun Deng, Ryumei Nakada, James Zou, and Linjun Zhang. The power of contrast for feature learning: A theoretical analysis. *Journal of Machine Learning Research*, 24(330):1–78, 2023.

Li Jing, Pascal Vincent, Yann LeCun, and Yuandong Tian. Understanding dimensional collapse in contrastive self-supervised learning. *arXiv preprint arXiv:2110.09348*, 2021.

Prannay Khosla, Piotr Teterwak, Chen Wang, Aaron Sarna, Yonglong Tian, Phillip Isola, Aaron Maschinot, Ce Liu, and Dilip Krishnan. Supervised contrastive learning. *Advances in neural information processing systems*, 33:18661–18673, 2020.

Byoungjip Kim, Jinho Choo, Yeong-Dae Kwon, Seongho Joe, Seungjai Min, and Youngjune Gwon. Selfmatch: Combining contrastive self-supervision and consistency for semi-supervised learning. *arXiv preprint arXiv:2101.06480*, 2021.

Alex Krizhevsky, Geoffrey Hinton, et al. Learning multiple layers of features from tiny images. 2009.

Phuc H Le-Khac, Graham Healy, and Alan F Smeaton. Contrastive representation learning: A framework and review. *Ieee Access*, 8:193907–193934, 2020.

Doyup Lee, Sungwoong Kim, Ildoo Kim, Yeongjae Cheon, Minsu Cho, and Wook-Shin Han. Contrastive regularization for semi-supervised learning. In *Proceedings of the IEEE/CVF conference on computer vision and pattern recognition*, pp. 3911–3920, 2022.

Alexander C Li, Alexei A Efros, and Deepak Pathak. Understanding collapse in non-contrastive siamese representation learning. In *European Conference on Computer Vision*, pp. 490–505. Springer, 2022.

Junnan Li, Caiming Xiong, and Steven CH Hoi. Comatch: Semi-supervised learning with contrastive graph regularization. In *Proceedings of the IEEE/CVF international conference on computer vision*, pp. 9475–9484, 2021.

Song Mei, Andrea Montanari, and Phan-Minh Nguyen. A mean field view of the landscape of two-layer neural networks. *Proceedings of the National Academy of Sciences*, 115(33):E7665–E7671, 2018.

Linghuan Meng and Chuang Wang. Training dynamics of nonlinear contrastive learning model in the high dimensional limit. *IEEE Signal Processing Letters*, 2024.

Grégoire Mialon, Quentin Garrido, Hannah Lawrence, Danyal Rehman, Yann LeCun, and Bobak Kiani. Self-supervised learning with lie symmetries for partial differential equations. *Advances in Neural Information Processing Systems*, 36:28973–29004, 2023.

Aaron van den Oord, Yazhe Li, and Oriol Vinyals. Representation learning with contrastive predictive coding. *arXiv preprint arXiv:1807.03748*, 2018.

Kendrick Shen, Robbie M Jones, Ananya Kumar, Sang Michael Xie, Jeff Z HaoChen, Tengyu Ma, and Percy Liang. Connect, not collapse: Explaining contrastive learning for unsupervised domain adaptation. In *International conference on machine learning*, pp. 19847–19878. PMLR, 2022.

Ankit Singh. Clda: Contrastive learning for semi-supervised domain adaptation. *Advances in Neural Information Processing Systems*, 34:5089–5101, 2021.

Yonglong Tian, Chen Sun, Ben Poole, Dilip Krishnan, Cordelia Schmid, and Phillip Isola. What makes for good views for contrastive learning? *Advances in neural information processing systems*, 33:6827–6839, 2020.

Laurens Van der Maaten and Geoffrey Hinton. Visualizing data using t-sne. *Journal of machine learning research*, 9(11), 2008.

Tongzhou Wang and Phillip Isola. Understanding contrastive representation learning through alignment and uniformity on the hypersphere. In *International conference on machine learning*, pp. 9929–9939. PMLR, 2020.

Zixin Wen and Yuanzhi Li. The mechanism of prediction head in non-contrastive self-supervised learning. *Advances in Neural Information Processing Systems*, 35:24794–24809, 2022.

Zhi-Qin John Xu, Yaoyu Zhang, Tao Luo, Yanyang Xiao, and Zheng Ma. Frequency principle: Fourier analysis sheds light on deep neural networks. *arXiv preprint arXiv:1901.06523*, 2019a.

Zhi-Qin John Xu, Yaoyu Zhang, and Yanyang Xiao. Training behavior of deep neural network in frequency domain. In *Neural Information Processing: 26th International Conference, ICONIP 2019, Sydney, NSW, Australia, December 12–15, 2019, Proceedings, Part I 26*, pp. 264–274. Springer, 2019b.

Fan Yang, Kai Wu, Shuyi Zhang, Guannan Jiang, Yong Liu, Feng Zheng, Wei Zhang, Chengjie Wang, and Long Zeng. Class-aware contrastive semi-supervised learning. In *Proceedings of the IEEE/CVF Conference on Computer Vision and Pattern Recognition*, pp. 14421–14430, 2022.

Chaoning Zhang, Kang Zhang, Chenshuang Zhang, Trung X Pham, Chang D Yoo, and In So Kweon. How does simsiam avoid collapse without negative samples? a unified understanding with self-supervised contrastive learning. *arXiv preprint arXiv:2203.16262*, 2022a.

Yuhang Zhang, Xiaopeng Zhang, Jie Li, Robert C Qiu, Haohang Xu, and Qi Tian. Semi-supervised contrastive learning with similarity co-calibration. *IEEE Transactions on Multimedia*, 25:1749–1759, 2022b.

A APPENDIX

In the appendix, we present the proofs of that are missing in the main manuscript.

A.1 INTERPRETATION OF VICREG AND BYOL

In this section, we show that two other popular methods related to deep learning models for learning dataset invariance exhibit a similar phenomenon as shown in Proposition 2.1, namely that the loss function itself is ill-posed. First, consider the VICReg Bardes et al. (2021) loss. Given a data distribution $\mu \in \mathbb{P}(\mathbb{R}^D)$ and a distribution for the perturbation functions ν, VICReg minimizes

$$\begin{aligned}\min_{f:\mathbb{R}^D\to\mathbb{R}^d} \mathbb{E}_{f,g\sim\nu}\mathbb{E}_{x_1,\cdots,x_n\sim\mu}\frac{\lambda_1}{n}\sum_{i=1}^{n}\|f(f(x_i)) - f(g(x_i))\|^2 \\ + \lambda_2\Big(v(f(f(x_1)),\cdots,f(f(x_n))) + v(f(g(x_1)),\cdots,f(g(x_n)))\Big) \\ + \lambda_3\Big(c(f(f(x_1)),\cdots,f(f(x_n))) + c(f(g(x_1)),\cdots,f(g(x_n)))\Big)\end{aligned}$$

where λ_1, λ_2, and λ_3 are hyperparameters. The first term ensures the invariance of f with respect to perturbation functions from ν, v maintains the variance of each embedding dimension, and c regularizes the covariance between pairs of embedded points towards zero. Suppose f is an invariant embedding map such that $f(T(x)) = f(x)$ for all $T \sim \nu$. Then, the above minimization problem becomes

$$\begin{aligned}
&\min_{f:\mathbb{R}^D\to\mathbb{R}^d} \mathbb{E}_{f,g\sim\nu}\mathbb{E}_{x_1,\cdots,x_n\sim\mu}\lambda_2\Big(v(f(x_1),\cdots,f(x_n))+v(f(x_1),\cdots,f(x_n))\Big)\\
&\qquad\qquad\qquad\qquad + \lambda_3\Big(c(f(x_1),\cdots,f(x_n))+c(f(x_1),\cdots,f(x_n))\Big)\\
&= \min_{f:\mathbb{R}^D\to\mathbb{R}^d} \mathbb{E}_{y_1,\cdots,y_n\sim f_\#\mu}\lambda_2\Big(v(y_1,\cdots,y_n)+v(y_1,\cdots,y_n)\Big)\\
&\qquad\qquad\qquad\qquad + \lambda_3\Big(c(y_1,\cdots,y_n)+c(y_1,\cdots,y_n)\Big)
\end{aligned}$$

Similar to the result in Proposition 2.1, the invariance term vanishes. This minimization can now be expressed as a minimization over the embedded distribution:

$$\begin{aligned}
&\min_{\rho\in\mathbb{P}(\mathbb{R}^d)} \mathbb{E}_{y_1,\cdots,y_n\sim\rho}\lambda_2\Big(v(y_1,\cdots,y_n)+v(y_1,\cdots,y_n)\Big)\\
&\qquad\qquad\qquad + \lambda_3\Big(c(y_1,\cdots,y_n)+c(y_1,\cdots,y_n)\Big)
\end{aligned}$$

This shows that given an invariant map f, the minimization problem becomes completely independent of the input data μ, thus demonstrating the same ill-posedness as the NT-Xent loss in Proposition 2.1.

Now, consider the loss function from BYOL Grill et al. (2020). Given a data distribution $\mu \in \mathbb{P}(\mathbb{R}^D)$ and a distribution for the perturbation functions ν, the loss takes the form

$$\min_{f,q} \mathbb{E}_{f,g\sim\nu}\mathbb{E}_{x\sim\mu}\|q(f(T(x))) - f(T'(x))\|^2$$

where $q : \mathbb{R}^d \to \mathbb{R}^d$ is an auxiliary function designed to prevent f from collapsing all points x to a constant in $\mathbb{R}^d$. Similar to the previous case, if we assume an invariant map f, the above problem becomes

$$\min_{f,q} \mathbb{E}_{x\sim\mu}\|q(f(x)) - f(x)\|^2 = \min_{f,q} \mathbb{E}_{y\sim f_\#\mu}\|q(y) - y\|^2$$

where the second equality follows from a change of variables. Again, this minimization problem can be written with respect to the embedded distribution as:

$$\min_{\rho\in\mathbb{P}(\mathbb{R}^d),q} \mathbb{E}_{y\sim\rho}\|q(y) - y\|^2$$

This again shows that once the invariant map is considered, the minimization problem becomes completely independent of the input data μ, highlighting the ill-posedness of the cost function.

A.2 FURTHER ANALYSIS OF THE STATIONARY POINTS OF EQUATION (4)

From the modified formulation eq. (4), we can define a minimizer that minimizes the function $L(f)$ on a constraint set $\mathcal{C} = \{f : \mathbb{R}^D \to \mathbb{R}^d\}$. The following proposition provides insight into the minimizer of eq. (4). The proof is provided in the appendix.

Proposition A.1. *This proposition describes three different possible local minimizers of eq.* (4) *that satisfy the Euler-Lagrange equation in eq.* (6).

1. *Any map $f : \mathbb{R}^D \to \mathbb{R}^d$ that maps to a constant, such that*

$$f(x) = c \in \mathbb{R}^d, \quad \forall x \in \mathcal{M}.$$

2. *In addition to the condition in eq.* (5)*, suppose the attraction and repulsion similarity functions $a : \mathbb{R}_{\geq 0} \to \mathbb{R}$ and $r : \mathbb{R}_{\geq 0} \to \mathbb{R}$ satisfy the following properties:*

   (a) *Each function is maximized at 0, where its value is 1.*
   (b) *Each function satisfies $\lim_{t\to\infty} a(t) = 0$ and $\lim_{t\to\infty} ta'(t) = 0$.*

   Let f be a map invariant to $\mathcal{T}$. Consider a sequence of maps $\{f_k\}$ such that

$$f_k(x) = kf(x), \quad \forall x \in \mathcal{M}, \forall k \in \mathbb{N}.$$

   The limit $f_* = \lim_{k\to\infty} f_k$ satisfies the Euler-Lagrange equation eq. (6).

Proof of Proposition A.1. If f is a constant function, it is trivial that it satisfies eq. (6).

Let us prove the second part of the proposition. From the Euler-Lagrange equation in eq. (6), by plugging in f_k and using the fact that f is invariant to $\mathcal{T}$, the Euler-Lagrange equation can be simplified to

$$\int_{\mathbb{R}^D} \left(\Psi'(G(f_k, \mathrm{Id}, x)) + \Psi'(G(f_k, \mathrm{Id}, y))\right) r'_{f_k}(x, y) \langle f_k(x) - f_k(y), h(x)\rangle \, d\mu(y)$$

for any $h : \mathbb{R}^D \to \mathbb{R}^d$. Using the invariance of f_k, we have

$$= \int_{\mathbb{R}^D} \Big(\Psi'(G(f_k, \mathrm{Id}, x)) + \Psi'(G(f_k, \mathrm{Id}, y))\Big) \Big(k r'_{f_k}(x, y)\Big) \langle f(x) - f(y), h(x)\rangle \, d\mu(y). \tag{22}$$

Furthermore, by the assumptions on the function r,

$$k r'_{f_k}(x, y) = k r'\left(\frac{k^2 \|f(x) - f(y)\|^2}{2}\right) \to 0, \quad \text{as } k \to \infty$$

$$\Psi'(G(f_k, \mathrm{Id}, x)) = \Psi'\left(\mathbb{E}_{z\sim\mu} r\left(\frac{k^2\|f(x) - f(z)\|^2}{2}\right)\right) \to \Psi'(0), \quad \text{as } k \to \infty.$$

Thus, eq. (22) converges to 0 as $k \to \infty$. This proves the theorem. $\square$

A.3 PROOF OF THEOREM 3.2

First, we prove Theorem 3.2, which characterizes the stationary points of the loss function. After the proof, we demonstrate that by considering an additional condition on the direction of the second variation at the stationary points, it is the second variation is strictly positive, thereby showing that the stationary point is a local minimizer under this condition.

Proof of Theorem 3.2. We consider the following problem:

$$\min_{f:\mathbb{R}^D \to \mathbb{S}^{d-1}} L(f), \tag{23}$$

where L is a loss function defined in eq. (4). The problem in eq. (23) can be reformulated as a constrained minimization problem:

$$\min_{\substack{f:\mathbb{R}^D \to \mathbb{R}^d \\ \|f\|=1}} L(f).$$

By relaxing the the constraint for $\|f\| = 1$, we can derive the lower bound such that

$$\min_{\substack{f:\mathbb{R}^D \to \mathbb{R}^d \\ \|f\|=1}} L(f) \geq \min_{\substack{f:\mathbb{R}^D \to \mathbb{R}^d \\ \int_{\mathbb{R}^D} \|f\| d\mu = 1}} L(f).$$

Note that since the constraint sets satisfy $\{\|f\| = 1\} \subset \{\int_{\mathbb{R}^D} \|f\| d\mu = 1\}$, the stationary point from from the latter constraint set is also the stationary point of the prior set.

By introducing the Lagrange multiplier λ for the constraint, we can convert the minimization problem into a minimax problem:

$$\min_{f:\mathbb{R}^D \to \mathbb{R}^d} \max_{\lambda \in \mathbb{R}} \left[L(f) + \lambda \mathbb{E}_{x\sim\mu}(1 - \|f(x)\|)\right]. \tag{24}$$

Using the Euler-Lagrange formulation in eq. (6), we can derive the Euler-Lagrange equation for the above problem, incorporating the Lagrange multiplier. To show that f is a minimizer of the problem in eq. (24), we need to demonstrate that there exists $\lambda \in \mathbb{R}$ such that the following equation holds:

$$\int_{\mathbb{R}^D} \left[\Psi'(G(f, x)) + \Psi'(G(f, y))\right] \eta'_f(x, y)(f(x) - f(y)) \, d\mu(y) - \lambda \frac{f(x)}{\|f(x)\|} = 0,$$

for all $x \in \mathcal{M}$. Note that since f is an invariant map, f disappears and $\eta_f(x, f(x)) = 1$. Furthermore, since f maps onto $\mathbb{S}^{d-1}$, we have $\|f(x)\| = 1$ for all $x \in \mathbb{R}^D$. Additionally, using the change of variables, we obtain

$$\lambda = C \int_{\mathbb{S}^{d-1}} r'(|x - y|^2/2)(x - y) \, df_{\#}\mu(y), \tag{25}$$

where C is defined as $C = \Psi'(\mathbb{E}_{z\sim f_{\#}\mu}\left[r(|x_0 - z|^2/2)\right])$ for $x_0 \sim f_{\#}\mu$. Given that the function

$$h(x, y) = r'(|x - y|^2/2)(x - y)$$

is an anti-symmetric function, by the assumption on $f_{\#}\mu$ in eq. (8), the integral on the right-hand side of eq. (25) is constant for all $x \sim f_{\#}\mu$. Therefore, by defining λ as in eq. (25), this proves the lemma. ☐

Now that we have identified the characteristics required for embedding maps to be stationary points, the next lemma shows that the second variation at this stationary point, in a specific direction h, is positive. This demonstrates that the stationary point is indeed a local minimizer along this particular direction.

Lemma A.2. *Fix $\tau > 0$ and define $\eta_f(x, y) = e^{-\|f(x)-f(y)\|^2/2\tau}$. Let $f : \mathbb{R}^D \to \mathbb{S}^{d-1}$ be an embedding map such that the embedded distribution $f_{\#}\mu = \sum_{i=1}^{n} \delta_{x_i}$ is a discrete measure on $\mathbb{S}^{d-1}$, satisfying that the number of points $n = Km$, where K is the number of cluster centers $\{\xi_i\}_{i=1}^{K}$ and m is some positive integer. Moreover, the points satisfy the condition:*

$$x_i = \xi_{\lfloor i/K\rfloor+1} \quad \text{for } i \in [\![n]\!]. \tag{26}$$

Furthermore, let $\sigma > 0$ be a positive constant satisfying $\sigma > 3K^2\tau$. Then,

$$\delta^2 L(f)(h, h) > 0$$

for any $h : \mathbb{R}^D \to \mathbb{R}^d$ satisfying $f + h \in \mathbb{S}^{d-1}$ and

$$\Big(\langle f(\xi_i) - f(\xi_j), h(\xi_i) - h(\xi_j)\rangle\Big)^2 \geq \sigma\|h(\xi_i) - h(\xi_j)\|^2. \tag{27}$$

Proof. Let $f : \mathbb{R}^D \to \mathbb{R}^d$ be an invariant embedding map. From the proof of **??**, the first variation takes the form

$$\int_{\mathbb{R}^D} \Psi'(G(f, x)) \int_{\mathbb{R}^D} \eta'_f(x, y)\langle f(x) - f(y), h(x) - h(y)\rangle d\mu(y)d\mu(x).$$

The second variation takes the form

$$\begin{aligned}
&\int_{\mathbb{R}^D} \Psi''(G(f, x)) \left(\int_{\mathbb{R}^D} \eta'_f(x, y)\langle f(x) - f(y), h(x) - h(y)\rangle d\mu(y)\right)^2 d\mu(x)\\
&+ \int_{\mathbb{R}^D} \Psi'(G(f, x)) \int_{\mathbb{R}^D} r''_f(x, y)\Big(\langle f(x) - f(y), h(x) - h(y)\rangle\Big)^2 d\mu(y)d\mu(x)\\
&+ \int_{\mathbb{R}^D} \Psi'(G(f, x)) \int_{\mathbb{R}^D} \eta'_f(x, y)\|h(x) - h(y)\|^2 d\mu(y)d\mu(x).
\end{aligned}$$

For simplicity, let us choose explicit forms for Ψ and r. The proof will be general enough to apply to any Ψ and r that satisfy the conditions mentioned in the paper. Let $\Psi(t) = \log(1 + t/2)$ and $r(t) = e^{-t/(2\tau)}$. With these choice of functions and by the change of variables,

$$\begin{aligned}
= &-\frac{1}{\tau^2}\int_{\mathbb{S}^{d-1}} \left(\frac{1}{1 + G(x)^2/2}\right)^2 \left(\int_{\mathbb{S}^{d-1}} e^{-\|x-y\|^2/(2\tau)}\langle x - y, T'(x) - T'(y)\rangle df_{\#}\mu(y)\right)^2 df_{\#}\mu(x)\\
&+ \frac{1}{\tau^2}\int_{\mathbb{S}^{d-1}} \frac{1}{1 + G(x)^2/2}\int_{\mathbb{S}^{d-1}} e^{-\|x-y\|^2/(2\tau)}\Big(\langle x - y, T'(x) - T'(y)\rangle\Big)^2 df_{\#}\mu(y)df_{\#}\mu(x)\\
&- \frac{1}{\tau}\int_{\mathbb{S}^{d-1}} \frac{1}{1 + G(x)^2/2}\int_{\mathbb{S}^{d-1}} e^{-\|x-y\|^2/(2\tau)}\|T'(x) - T'(y)\|^2 df_{\#}\mu(y)df_{\#}\mu(x).
\end{aligned} \tag{28}$$

where $G(x) = \mathbb{E}_{y\sim f_{\#}\mu} e^{-\|x-y\|^2/(2\tau)}$ and $T'(x) = h(f^{-1}(x))$. By Jensen's inequality, we have

$$\begin{aligned}
&\left(\int_{\mathbb{S}^{d-1}} e^{-\|x-y\|^2/(2\tau)}\langle x - y, T'(x) - T'(y)\rangle df_{\#}\mu(y)\right)^2\\
&\leq \int_{\mathbb{S}^{d-1}} e^{-\|x-y\|^2/(2\tau)}\Big(\langle x - y, T'(x) - T'(y)\rangle\Big)^2 df_{\#}\mu(y).
\end{aligned}$$

Therefore, eq. (28) can be bounded below by

$$
\begin{aligned}
\geq & \frac{1}{\tau^2}\int_{\mathbb{S}^{d-1}} \frac{G(x)^2/2}{(1+G(x)^2/2)^2}\int_{\mathbb{S}^{d-1}} e^{-\|x-y\|^2/(2\tau)}\Big(\langle x-y, T'(x)-T'(y)\rangle\Big)^2 df_{\#}\mu(y)df_{\#}\mu(x)\\
&\qquad -\frac{1}{\tau}\int_{\mathbb{S}^{d-1}} \frac{1}{1+G(x)^2/2}\int_{\mathbb{S}^{d-1}} e^{-\|x-y\|^2/(2\tau)}\|T'(x)-T'(y)\|^2 df_{\#}\mu(y)df_{\#}\mu(x)\\
= & \frac{1}{\tau^2}\int_{\mathbb{S}^{d-1}} \frac{1}{1+G(x)^2/2}\int_{\mathbb{S}^{d-1}} e^{-\|x-y\|^2/(2\tau)}\\
&\qquad \left(\frac{G(x)^2}{2(1+G(x)^2/2)}\Big(\langle x-y, T'(x)-T'(y)\rangle\Big)^2 - \tau\|T'(x)-T'(y)\|^2\right) df_{\#}\mu(y)df_{\#}\mu(x).
\end{aligned}
$$

By the assumption on $f_{\#}\mu$ in eq. (26), the above can be written as

$$
\begin{aligned}
= & \frac{1}{n^2\tau^2}\sum_{i=1}^{n}\frac{1}{1+\widetilde{G}(x_i)^2/2}\sum_{\substack{j=1\\ j\neq i}}^{n} e^{-\|x_i-x_j\|^2/(2\tau)}\\
&\qquad \left(\frac{\widetilde{G}(x_i)^2}{2(1+G(x)^2/2)}\Big(\langle x_i-x_j, g(x_i)-g(x_j)\rangle\Big)^2 - \tau\|g(x_i)-g(x_j)\|^2\right)\\
= & \frac{m^2}{n^2\tau^2}\sum_{i=1}^{K}\frac{1}{1+\widetilde{G}(\xi_i)^2/2}\sum_{\substack{j=1\\ j\neq i}}^{K} e^{-\|\xi_i-\xi_j\|^2/(2\tau)}\\
&\qquad \left(\frac{\widetilde{G}(\xi_i)^2}{2(1+\widetilde{G}(\xi_i)^2/2)}\Big(\langle \xi_i-\xi_j, g(\xi_i)-g(\xi_j)\rangle\Big)^2 - \tau\|g(\xi_i)-g(\xi_j)\|^2\right)
\end{aligned}
\tag{29}
$$

If $K = 1$, the second variation becomes 0, and is therefore nonnegative. Now, suppose $K > 1$. We can bound $\widetilde{G}$ from below by

$$
\widetilde{G}(\xi_i) = \frac{1}{K}\sum_{k=1}^{K} e^{-\|\xi_i-\xi_k\|^2/(2\tau)} \geq \frac{1}{K}. \tag{30}
$$

Furthermore, from the condition in eq. (27), we have

$$
\Big(\langle \xi_i-\xi_j, g(\xi_i)-g(\xi_j)\rangle\Big)^2 \geq \sigma\|g(\xi_i)-g(\xi_j)\|^2 \tag{31}
$$

for some positive constant $\sigma > 0$. Combining eq. (30) and eq. (31), we can bound eq. (29) from below by

$$
\geq \frac{1}{K^2\tau^2}\sum_{i=1}^{K}\frac{1}{1+\widetilde{G}(\xi_i)^2/2}\sum_{\substack{j=1\\ j\neq i}}^{K} e^{-\|\xi_i-\xi_j\|^2/(2\tau)}\Big(\frac{\sigma}{3K^2}-\tau\Big)\|g(\xi_i)-g(\xi_j)\|^2.
$$

By the condition on σ, the above quantity is strictly greater than zero. This concludes the proof of the lemma.

□

A.4 PROOF OF PROPOSITION 4.1

Proof. The gradient of $\mathcal{L}$ is given by

$$
\nabla\mathcal{L}(w) = \frac{1}{n}\sum_{i=1}^{n}\sum_{k=1}^{d}\nabla_{y^k}L(f(w,x_i))\nabla_w f^k(w,x_i) \tag{32}
$$

where $\nabla_{y^k}L(f(w,x_i))$ is a gradient of L with respect to y_k coordinate. For simplicity of notation, let us denote by

$$
f_i^k = f^k(w,x_i), \quad L_i = L(f(w,x_i)).
$$

Thus, eq. (32) can be rewritten as

$$\nabla \mathcal{L}(w) = \frac{1}{n}\sum_{i=1}^{n}\sum_{k=1}^{d} \nabla_{y^k} L_i \nabla_w f_i^k \tag{33}$$

By the definition of the loss function in eq. (9), $w(t)$ satisfies the gradient flow such that

$$\dot{w}(t) = -\nabla \mathcal{L}(w). \tag{34}$$

Thus, the solution of the above ODE converges to the local minimizer of $\mathcal{L}$ as t grows.

For each $i \in [\![n]\!]$ and $k \in [\![d]\!]$, denote by

$$z_i^k(t) = f_i^k(t).$$

Let us compute the time derivative of z_i^k. Using a chain rule, eq. (33) and eq. (34),

$$\dot{z}_i^k(t) = \nabla_w f_i^k \cdot \dot{w}(t) = -\nabla_w f_i^k \cdot \nabla \mathcal{L}(w) = -\frac{1}{n}\sum_{j=1}^{m}\sum_{l=1}^{d} \nabla_w f_i^k \cdot \nabla_w f_j^l \, \nabla_{y^l} L_j. \tag{35}$$

Using eq. (12), eq. (35), $\dot{z}_i(t)$ can be written as

$$\dot{z}_i(t) = -\frac{1}{n}\sum_{j=1}^{n} K_{ij} \nabla L_j(t).$$

This completes the proof. □

A.5 PROOF OF THEOREM 4.2

Proof. Consider the gradient descent iterations in eq. (14). Suppose f is invariant to the perturbation from ν at b-th iteration, that is we have $f(w^{(b)}, f(x)) = f(w^{(b)}, x)$ for all $x \sim \mu$ and $T \sim \nu$. We want to show that, given an invariant embedding map $f(w^{(b)}, \cdot)$, it remains invariant after iteration b. From the gradient formulation of the loss function in Proposition 3.1, we have

$$\nabla L(f(w^{(b)}, x)) = -\int_{\mathbb{R}^D} \Psi'(x, y)(f(w^{(b)}, x) - f(w^{(b)}, y)) \, d\mu(y),$$

where $\Psi'(x, y) = \Big(\Psi'(G(f(w^{(b)}, \cdot), x)) + \Psi'(G(f(w^{(b)}, \cdot), y))\Big)\eta'_{f(w^{(b)}, \cdot)}(x, y)$.

From the gradient descent formulation in eq. (14), we have

$$f(w^{(b+1)}, f(x_i)) = f(w^{(b)}, f(x_i)) - \sigma \nabla L(f(w^{(b)}, f(x_i))),$$

which gives

$$f(w^{(b+1)}, f(x_i)) = f(w^{(b)}, f(x_i)) + \sigma \int_{\mathbb{R}^D} \Psi'(x, y)(f(w^{(b)}, f(x_i)) - f(w^{(b)}, y)) \, d\mu(y),$$

and since $f(w^{(b)}, f(x_i)) = f(w^{(b)}, x_i)$ by invariance, this simplifies to

$$f(w^{(b+1)}, x_i) - \sigma \nabla L(f(w^{(b)}, x_i)) = f(w^{(b+1)}, x_i),$$

which shows that $f(w^{(b+1)}, x_i)$ is invariant for all $i \in [\![n]\!]$. Therefore, the embedding map remains invariant throughout the optimization process.

Now, consider the gradient descent iteration with a neural network in eq. (15). Suppose f is invariant to perturbations from ν and satisfies

$$\nabla_w f(w^{(b)}, f(x)) = \nabla_w f(w^{(b)}, x), \quad \forall x \sim \mu, f \sim \nu. \tag{36}$$

Denote the kernel matrix function K_{ij} given a perturbation function $T \sim \nu$ as

$$(K_{ij}(w^{(b)}, f))^{kl} = (\nabla_w f^k(w^{(b)}, f(x_i)))^\top (\nabla_w f^l(w^{(b)}, f(x_j))).$$

Then, we have

$$\begin{aligned} f(w^{(b+1)}, f(x_i)) &= f(w^{(b)}, f(x_i)) - \frac{\sigma}{n}\sum_{j=1}^{n} K_{ij}(w^{(b)}, f)\nabla L(f(w^{(b)}, f(x_i))) \\ &= f(w^{(b)}, x_i) - \frac{\sigma}{n}\sum_{j=1}^{n} K_{ij}(w^{(b)}, \mathrm{Id})\nabla L(f(w^{(b)}, x_i)) \\ &= f(w^{(b+1)}, x_i). \end{aligned}$$

Thus, if f is invariant at the b-th iteration, it remains invariant. However, note that this result no longer holds if the condition in eq. (36) fails, meaning that f is not invariant for $b+1$-th iteration. This completes the proof. $\square$

A.6 PROOF OF PROPOSITION 4.3

Proof. We describe the matrices $A \in \mathbb{R}^{Md\times d}$ and $B \in \mathbb{R}^{Md\times D}$ as follows:

$$A = \begin{pmatrix} | & | & \cdots & | \\ a^1 & a^2 & \cdots & a^d \\ | & | & \cdots & | \end{pmatrix} = \begin{pmatrix} - & a_1 & - \\ & \vdots & \\ - & a_{Md} & - \end{pmatrix} = \begin{pmatrix} a_1^1 & \cdots & a_1^d \\ \vdots & \cdots & \vdots \\ a_{Md}^1 & \cdots & a_{Md}^d \end{pmatrix},$$

$$B(t) = \begin{pmatrix} | & | & \cdots & | \\ b^1(t) & b^2(t) & \cdots & b^D(t) \\ | & | & \cdots & | \end{pmatrix} = \begin{pmatrix} - & b_1(t) & - \\ & \vdots & \\ - & b_{Md}(t) & - \end{pmatrix} = \begin{pmatrix} b_1^1(t) & \cdots & b_1^D(t) \\ \vdots & \cdots & \vdots \\ b_{Md}^1(t) & \cdots & b_{Md}^D(t) \end{pmatrix}.$$

In this notation, a^k and b^k are Md-dimensional column vectors, a_p and b_p are d- and D-dimensional row vectors, and a_p^k and b_p^k are scalars.

We can write f^k with respect to a_i^k and b_i^k.

$$f^k(B, x) = (a^k)^\top \sigma(Bx) = \sum_{i=1}^{Md} a_i^k \sigma\Big(b_i x\Big) = \frac{1}{\sqrt{M}} \sum_{i=(k-1)M+1}^{kM} \sigma\Big(b_i x\Big)$$

where the last equality uses the definition of a matrix A in eq. (19). By differentiating with respect to b_i^l, we can derive explicit forms for the gradient of f^k with respect to a weight matrix B.

$$\begin{aligned} \nabla_w f^k(B, x) &= \Big(a^k \odot \sigma'(Bx)\Big)x^\top \\ &= \begin{pmatrix} a_1^k\sigma'(b_1x)x^1 & \cdots & a_1^k\sigma'(b_1x)x^D \\ \vdots & \ddots & \vdots \\ a_M^k\sigma'(b_Mx)x^1 & \cdots & a_M^k\sigma'(b_Mx)x^D \end{pmatrix} \\ &= \frac{1}{\sqrt{M}} \begin{pmatrix} 0 & \cdots & 0 \\ \vdots & \ddots & \vdots \\ 0 & \cdots & 0 \\ \sigma'(b_1x)x^1 & \cdots & \sigma'(b_1x)x^D \\ \vdots & \ddots & \vdots \\ \sigma'(b_Mx)x^1 & \cdots & \sigma'(b_Mx)x^D \\ 0 & \cdots & 0 \\ \vdots & \ddots & \vdots \\ 0 & \cdots & 0 \end{pmatrix} \in \mathbb{R}^{Md\times D} \end{aligned}$$

where the row index of nonzero entries ranges from $(k-1)M+1$ to kM.

Define an inner product such that for $h \in \mathbb{R}^{Md\times D}$

$$\langle \nabla_w f^k(B, x), h\rangle, \quad k \in [\![D]\!].$$

Now we are ready to show the explicit formula of the inner product $\langle \nabla_w f^k, \nabla_w f^l \rangle$.

$$\langle \nabla_w f^k(B, x_i), \nabla_w f^l(B, x_j) \rangle = \frac{\mathbb{1}_{k=l}}{M} (x_i^\top x_j) \sum_{p=(k-1)M+1}^{kM} \sigma'(b_p x_i) \sigma'(b_p x_j)$$

where $\mathbb{1}_{k=l}$ is an indicator function that equals 1 if $k = l$ and 0 otherwise. Therefore, the kernel matrix takes the form

$$(K^{kl})_{ij} = \frac{\mathbb{1}_{k=l}}{M} (x_i^\top x_j) \sum_{p=(k-1)M+1}^{kM} \sigma'(b_p x_i) \sigma'(b_p x_j).$$

□

Proof of Theorem 4.5. Using the definition of a function γ in Theorem 4.5 and using the structure of the dataset $\{x_i\}$ in eq. (16), consider x_i and x_j in $\gamma(i)$-th cluster and $\gamma(j)$-th cluster respectively. Since the dataset is sampled from a compactly supported data distribution and given the assumption that the activation function has bounded derivatives, we have

$$\begin{aligned} x_i^\top x_j &= \xi_{\gamma(i)}^\top \xi_{\gamma(j)} + O(\delta) = \mathbb{1}_{\gamma(i)=\gamma(j)} + O(\delta) \\ \sigma'(b_p x_i) &= \sigma'(b_p \xi_{\gamma(i)}) + O(\delta). \end{aligned}$$

Thus,

$$K_{ij}^{kl} = \frac{\mathbb{1}_{k=l}}{M} \xi_{\gamma(i)}^\top \xi_{\gamma(j)} \mathbb{1}_{\gamma(i)=\gamma(j)} \sum_{p=(k-1)M+1}^{kM} \sigma'(b_p \xi_{\gamma(i)}) \sigma'(b_p \xi_{\gamma(j)}) + O(\delta).$$

Combining all, we can write the kernel matrix K_{ij} as the following

$$K_{ij} = \mathbb{1}_{\gamma(i)=\gamma(j)} \|\xi_{\gamma(i)}\|^2 \boldsymbol{\beta}_{\gamma(i)} + O(\delta)$$

where $\boldsymbol{\beta}_i \in \mathbb{R}^{d \times d}$ ($i \in [\![n]\!]$) is a diagonal matrix defined as

$$\boldsymbol{\beta}_i = \begin{pmatrix} \beta_i^1 & 0 & \cdots & 0 \\ 0 & \beta_i^2 & \cdots & 0 \\ \vdots & \vdots & \ddots & \vdots \\ 0 & 0 & \cdots & \beta_i^d \end{pmatrix}$$

where $\beta_i^k \in \mathbb{R}$ ($k \in [\![d]\!]$) is defined as

$$\beta_i^k = \frac{1}{M} \sum_{p=(k-1)M+1}^{kM} \sigma'(b_p \xi_{\gamma(i)})^2. \tag{37}$$

Thus, from the gradient flow formulation in eq. (10), we have

$$\begin{aligned} \dot{z}_i(t) &= -\frac{1}{n} \sum_{j=1}^{n} K_{ij}(t) \nabla L_j(t) \\ &= -\frac{\|\xi_{\gamma(i)}\|^2}{n} \boldsymbol{\beta}_{\gamma(i)} \sum_{j \in \gamma(i)} \nabla L_j(t) + O(\delta) \\ &= -\frac{\|\xi_{\gamma(i)}\|^2}{n} (n_{\gamma(i)} - n_{\gamma(i)-1}) \boldsymbol{\beta}_{\gamma(i)} \nabla L(w(t), \xi_{\gamma(i)}) + O(\delta) \\ &= -\left(\frac{n_{\gamma(i)} - n_{\gamma(i)-1}}{n} \right) \|\xi_{\gamma(i)}\|^2 \boldsymbol{\beta}_{\gamma(i)} \nabla L(w(t), \xi_{\gamma(i)}) + O(\delta). \end{aligned}$$

□

B EXTRA NUEMRICAL RESULTS

In this section, we provide additional experimental results to validate Theorem 4.5, showing that neural network optimization influences training dynamics. Even when starting with the same random initialization of the embedded distribution, the training dynamics with neural networks are guided toward stationary points where the clustering structure is imposed. In contrast, vanilla gradient descent without neural network optimization is independent of the data structure.

The comparison of optimization processes with and without neural network training in 2D and 3D is shown, with the data distribution presented in (a) and (l). A 4-layer fully connected neural network was used in this experiment, demonstrating that the same behavior is observed even with different neural network architectures. The color of each point corresponds to its respective cluster. Rows 2 and 5 illustrate optimization with neural network training, starting from a random initial embedding and progressively revealing the clustering structure over iterations. Rows 3 and 6 show the optimization process using vanilla gradient descent without neural network training. Over time, the distribution converges to a uniformly dispersed arrangement, disregarding the clustering structure of the input data.

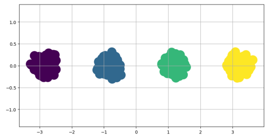

(a) Input data in 2D

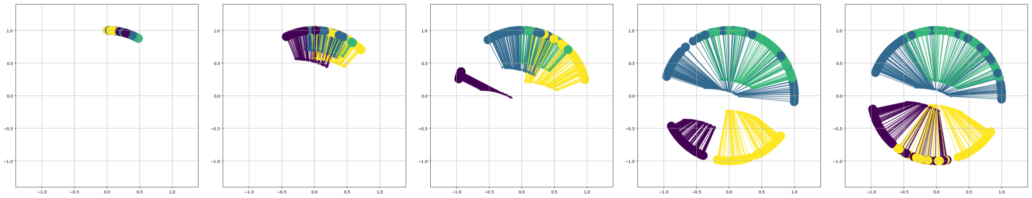

(b) It: 0 (c) It:70 (d) It: 80 (e) It: 100 (f) It: 500

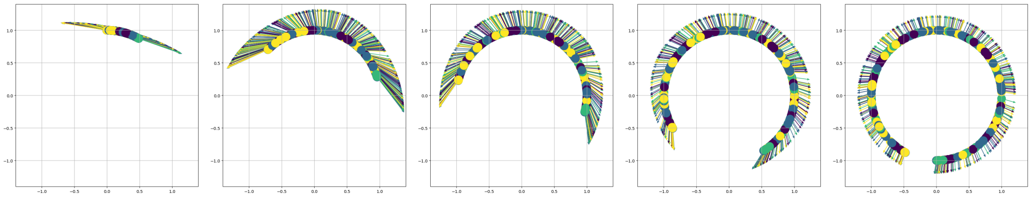

(g) It: 0 (h) It:50 (i) It: 200 (j) It: 400 (k) It: 800

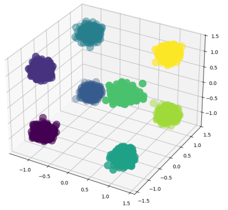

(l) Input data in 3D

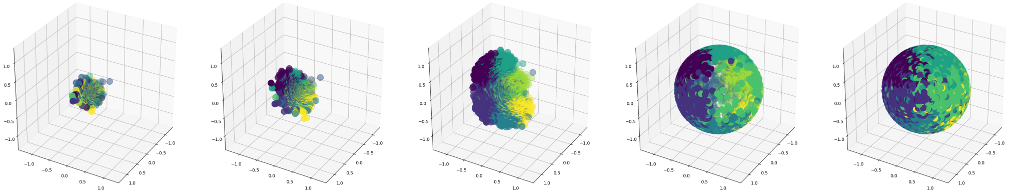

(m) It: 0 (n) It:700 (o) It: 1,000 (p) It: 1,500 (q) It: 2,000

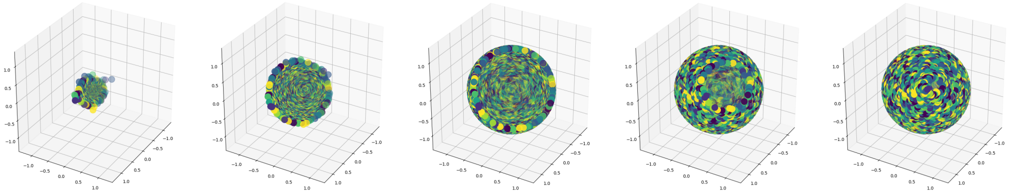

(r) It: 0 (s) It:50 (t) It: 400 (u) It: 1,000 (v) It: 2,000

Figure 5: This experiment compares the optimization processes with and without neural network training in 2D and 3D, with the data distribution depicted in (a) and (l). A 4-layer fully connected neural network demonstrates consistent outcome as in Figure 4. Each point's color indicates its cluster. Rows 2 and 5 show optimization with neural network training, starting from a random embedding and gradually revealing the clustering structure. In contrast, Rows 3 and 6 illustrate the optimization process using vanilla gradient descent, which converges to a uniformly dispersed arrangement, disregarding the input data's clustering structure.